International Scientific Journal
Environmental Science
http://environment.scientific-journal.com

$Fe_3O_4/SiO_2/CeO_2$ Core-Shell Magnetic Nanoparticles as Photocatalyst

Duangdao Channei
Department of Chemistry, Faculty of Science Chiang Mai University, Chiang Mai 50200, Thailand

Natda Wetchakun
Department of Physics and Materials Science, Faculty of Science Chiang Mai University, Chiang Mai 50200, Thailand

Burapat Inceesungvorn
Department of Chemistry, Faculty of Science Chiang Mai University, Chiang Mai 50200, Thailand

Sukon Phanichphant*
Materials Science Research Center, Faculty of Science Chiang Mai University, Chiang Mai 50200, Thailand
*E-mail: sphanichphant@yahoo.com

Abstract

The Fe_3O_4/CeO_2 magnetic photocatalyst was prepared by coating directly onto the surface of magnetic Fe_3O_4 particles. However a direct contact of CeO_2 onto the surface of magnetic Fe_3O_4 particles presented unfavorable heterojunction, thus the SiO_2 barrier layer between magnetic Fe_3O_4 and CeO_2 was prepared as a core-shell stucture to reduce the negative effect by combining three steps of the hydrothermal, sonochemical and homogeneous precipitation. The high resolution electron microscopy (HRTEM) confirmed that $Fe_3O_4/SiO_2/CeO_2$ core-shell magnetic nanoparticles exhibited core-shell structure including a magnetic Fe_3O_4 core, a SiO_2 middle layer and CeO_2 particle coating. The results of the photocatalytic activity revealed that the pseudo-first order rate constants for formic and oxalic acids degradation was increased in the following order: $Fe_3O_4/SiO_2/CeO_2$ core-shell magnetic nanoparticles> single-phase CeO_2> Fe_3O_4/CeO_2. SiO_2 middle layer and their surface properties may cause the good photocatalytic activity of the $Fe_3O_4/SiO_2/CeO_2$ core-shell magnetic nanoparticles. The possible mechanism of the photoexcited electron-hole separation and transport processes was proposed based on the obtained morphology via HRTEM morphology and UV-Vis DRS results. The $Fe_3O_4/SiO_2/CeO_2$ core-shell magnetic nanoparticles were compared and recovered in the consecutive cycles of use by external magnetic field. The material showed good stability with regards to photocatalytic performance for three cycles of use.

Key words:CeO_2; photocatalyst; core-shell structures; photocatalysis; magnetic photocatalyst

I. Introduction

Nowadays, water pollution is one of important environmental problems. The main source of water pollutant is an organic compound from industries, agricultures, houses, and research laboratories [1, 2]. Therefore, it is necessary to improve water quality and remove pollution from wastewater. Various physical-chemical techniques are available for the wastewater treatments. They include biological treatment (aerobic, anaerobic) [3] and physicochemical methods (activated carbon adsorption, emulsion liquid membrane, and ion exchanges), which have low reaction rates and take longer times [4–6]. The advanced oxidation processes (AOPs) is the novel method, which are very powerful in reducing heavy metals, decolorization, oxidization, mineralization and degrading organic pollutants [7,8]. Among AOPs, heterogeneous photocatalysis has been successfully employed for the degradation and transform the organic pollutant into less harmful substances based on the highly reactive oxidizing species hydroxyl radicals (OH•), which can attack organic pollutant in waste water and finally generating the nontoxic inorganic substances such as CO_2 and H_2O as a reaction products [9–11]. Many heterogeneous photocatalyst such as TiO_2, WO_3, and ZnO are widely used for water pollutant photodecomposition [12–14]. Apart of various semiconductor photocatalysts available, cerium dioxide (ceria, CeO_2) has attracted much attention due to its high activity, large stability to light illumination, low price, nontoxicity, and insoluble in water, which make CeO_2 an interesting photocatalyst [15,16]. In addition, CeO_2 is superior being used as a photocatalyst because of its easy

redox nature of $Ce^{4+/}Ce^{3+}$ couple transformation, which may support the charge carrier transfer to the catalyst surface [17]. In the photocatalytic testing process, catalysts powder is normally used as suspension form in photoreactor. The effective recovery process of the nanosized powders from the treated water suspension is still a challenge as such many researchers have been investigated about the chemical settling process for suspended catalyst separation such as centrifugation and filtration [18, 19]. However, some loss of catalyst during these separation processes is the major drawback, which requires coating the catalyst onto the support. Many researchers have coated photocatalyst onto the substrate such as glass, zeolite and other substrates in order to improve the separation efficiency but the coated catalyst on the support lack the high surface area required for effective catalysis [20–22]. The magnetic separation process is a new process that provides a very convenient approach for removing and recycling magnetic particles from the treated water by applying external magnetic fields [23,24]. Another advantage of core-shell structured composites is that they can improve the photocatalytic performance owing to the interactions between different components [25, 26].

The aims of this work include (i) developing a CeO_2 magnetic photocatalyst by coating CeO_2 on magnetic core (Fe_3O_4) and silica (SiO_2) layer via a wet-chemical process including hydrothermal, sonochemical and homogeneous precipitation methods; (ii) characterizing the physical and chemical properties, as well as study their photocatalytic performance by degrading formic and oxalic acids as the model organic compound; (iii) comparing the photocatalytic performance of $Fe_3O_4/SiO_2/CeO_2$ core-shell magnetic nanoparticls with single-phase CeO_2 and Fe_3O_4/CeO_2, and confirming their stability; (iv) proposing a mechanism of the photoexcited electron-hole separation and transport processes.

II. Materials and methods

A. Preparation of Fe_3O_4 magnetic core

The synthesis was carried out through a hydrothermal process. Typically, iron (III) chloride hexahydrate ($FeCl_3.6H_2O$) was dissolved in ethylene glycol, then sodium acetate trihydrate ($C_2H_3NaO_2.3H_2O$) was added to the mixed solution followed by polyethylene glycol (PEG) with molecular weights of 4,000 g/mol. The resulting mixture was stirred for 1 h, then transferred into a Teflon-lined stainless steel autoclave. The autoclave was sealed and the hydrothermal reaction was carried out at 200°C for 8 h. The product was washed with deionized water until washings were neutral. Finally, the Fe_3O_4 magnetic product was dried at 80ºC for 24 h for further use.

B. Preparation of Fe_3O_4/SiO_2 core-shell

Firstly, as-prepared Fe_3O_4 particles were dispersed in the mixture of tetraethyl orthosilicate (TEOS) and absolute ethanol (CH_2OH) under ultrasonication. The ammonia aqueous solution (NH_4OH) with a concentration of 25% was added in to the mixed solution and continued sonication for 3 h. The Fe_3O_4/SiO_2 core-shell product was collected by a centrifuge, washed with deionized water, and dried at 80°C for 24 h.

C. Preparation of single-phase CeO_2 nanoparticle

Single-phase CeO_2 was prepared by homogeneous precipitation and subsequent calcination process. Firstly, cerium nitrate hexahydrate ($Ce(NO_3)3.6H_2O$) was dissolved in 80% ethylene glycol solution ($C_2H_6O_2$) and kept under stirring at 50°C until a homogeneous solution was obtained. The color of solution change from purple towards a yellow color after 3.0 M ammonia solution (NH_4OH) was subsequently added to the mixed solution. Afterwards all the mixture was aged at 50°C for 12 h and then the purple suspension changed to a turbid yellow color once again. The suspension was washed with deionized water/ethanol, and then dried in a vacuum oven at 70°C for 24 h. Finally, the single-phase CeO_2 product was calcined at 500°C for 1 h.

D. Preparation of $Fe_3O_4/SiO_2/CeO_2$ core-shell magnetic nanoparticles

The $Fe_3O_4/SiO_2/CeO_2$ core-shell magnetic nanoapticles was synthesized by the homogeneous precipitation, similar to the method of single-phase CeO_2 preparation (section C) with slight modification. One difference is that the as-prepared Fe_3O_4/SiO_2 core-shell particle was added in to the mixed solution of cerium nitrate hexahydrate and 80% ethylene glycol solution before 3.0 M ammonia solution was introduced to the mixture.

E. Preparation of Fe_3O_4/CeO_2

In order to compare the photocatalytic activity with other prepared catalysts, Fe_3O_4/CeO_2 was prepared following the procedure described in section of CeO_2 preparation in the presence of Fe_3O_4 magnetic particles by dispersion Fe_3O_4 particle in the mixed solution of cerium nitrate hexahydrate and 80% ethylene glycol, then followed the preparation step as explained in section C.

III. Characteizations

The structure and mixed phase composition of the prepared samples were examined by X-ray powder diffraction (XRD; Philip X' Pert PRO PW

3719). High resolution transmission electron microscopy (HRTEM; JEM-2010, JEOL) was carried out in order to measure the morphology, particle size, and layer size of the prepared samples. Brunauer, Emmett, and Teller nitrogen adsorption method (BET, QuantachromeAutosorp 1 MP) was employed to calculate the specific surface area (SSA), pore size diameter, and pore volume. The magnetic hysteresis loops were recorded using a vibrating sample magnetometer (VSM; 7404, Lakeshore, USA) at room temperature. In order to estimate the band gap energies of the prepared samples, the optical properties were obtained from a Shimadzu UV-3010 spectrometer with integrating sphere attachment. X-ray photoelectron spectroscopy (XPS) was employed to characterize the chemical composition and valence state, as well as the shifted peaks in binding energy (MgKα, Kratos Axis Ultra DLD). The binding energy of the carbon (C 1s) line at 285 eV was fixed to calibrate and collected of other peaks according to the position of the C 1s signal.

IV. Measurement of photocatalytic activity

The photocatalytic activities of the prepared samples were measured using a spiral photoreactor system, which equipped with a UV light source and a conductivity monitor for carbon dioxide detection. Formic or oxalic acid (500 µg of carbon) was added to a photocatalyst suspension and measured the generated carbon dioxide as the organic photodegrades at 15 sec different time intervals. The photocatalytic degradation was assumed to be completed when there was no further change in conductivity. Finally, the rest amount of formic or oxalic acid after photocatalytic degradation was converted from the conductivity value using a calibration curve. In order to reuse the $Fe_3O_4/SiO_2/CeO_2$ core-shell magnetic nanoparticles in another test, these magnetic catalysts were magnetically recovered by placing an external magnetic field.

V. Results and discussion

The XRD pattern was carried out in order to study the structure and phase composition of the prepared samples. The XRD patterns of photocatalysts are compared in Fig. 1. All peaks of single-phase CeO_2 and Fe_3O_4 were matched well with the JCPDS file no.34-0394 and 15-7609 [27,28], respectively. Diffraction peak labels "M" denoted the Fe_3O_4 phase and CeO_2 phases denoted as "C". The diffraction peaks of Fe_3O_4/SiO_2 sample presented the same patterns with Fe_3O_4 indicating that the SiO_2 was amorphous. The successful coating of the CeO_2 on magnetic core Fe_3O_4 and Fe_3O_4/SiO_2 have been confirmed by the new peaks of CeO_2 phase in the XRD pattern.

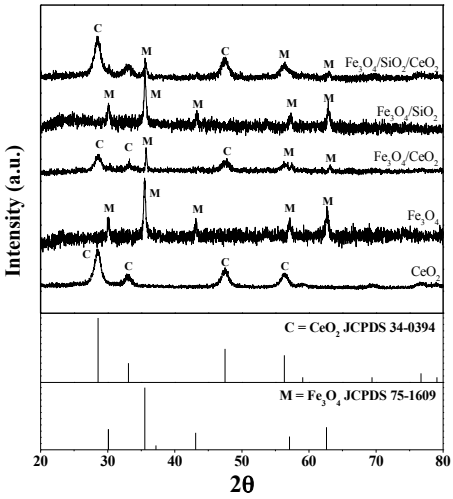

Fig. 1. The XRD patterns of CeO_2, Fe_3O_4, Fe_3O_4/CeO_2, Fe_3O_4/SiO_2, and $Fe_3O_4/SiO_2/CeO_2$ core-shell magnetic nanoparticles.

Magnetic properties of the prepared samples were measured by VSM at room temperature as shown in Fig. 2. Since the magnetic hysteresis loop was not appeared in the curve, thus the prepared Fe_3O_4 displayed the superparamagnetism behavior with 52.1290 emu/g saturation intensity [29]. After coated with SiO_2 and CeO_2, the saturation magnetization (Ms) of Fe_3O_4 gradually decreased in the order of Fe_3O_4 (52.1290 emu/g)> Fe_3O_4/CeO_2 (43.0262 emu/g)> Fe_3O_4/SiO_2 (40.1530 emu/g)> $Fe_3O_4/SiO_2/CeO_2$ (8.9046 emu/g). This is possibly because the non-magnetic coating layer SiO_2 and/or CeO_2 was coated over the surface of Fe_3O_4 magnetic core as a result of decreasing subsequences in magnetism and quenching of surface magnetic moments [30]. However, the magnetism of $Fe_3O_4/SiO_2/CeO_2$ core-shell magnetic nanoparticles (Fig. 2d) is still strong enough to be magnetically separated by applying an external magneticfield in the process of photocatalysts separation from the treated suspension.

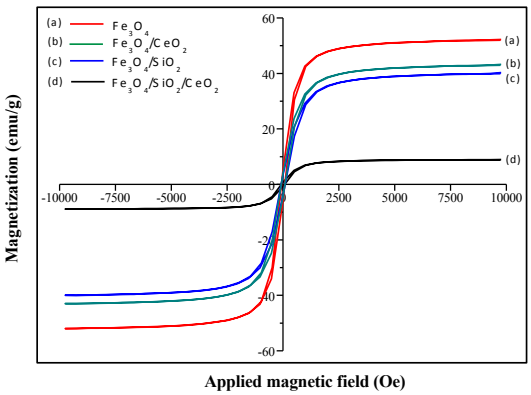

Fig. 2. Room-temperature magnetization curve of (a) Fe_3O_4, (b) Fe_3O_4/CeO_2, (C) Fe_3O_4/SiO_2, and (d) $Fe_3O_4/SiO_2/CeO_2$ core-shell magnetic nanoparticles.

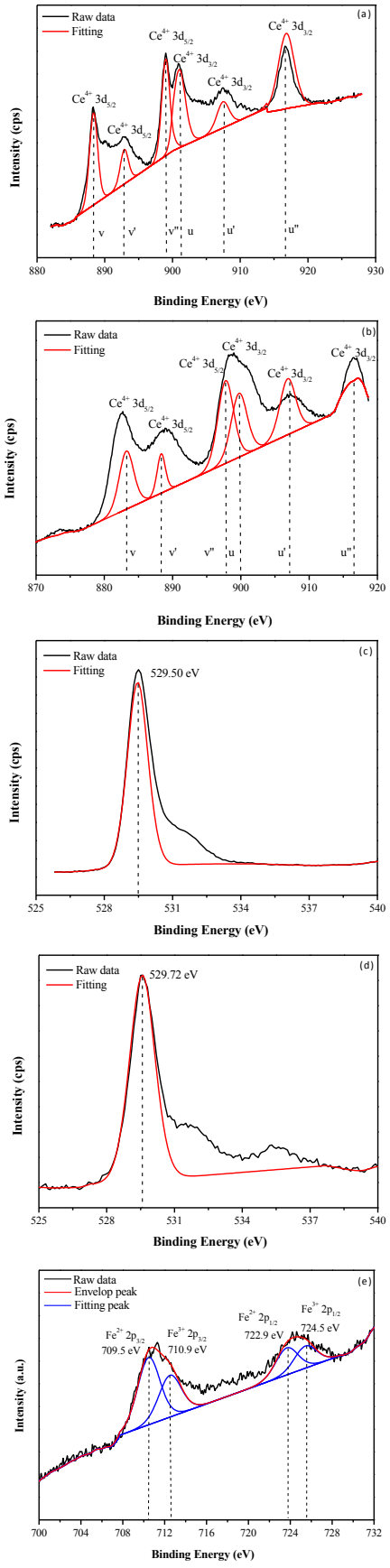

Fig. 3. The XPS spectra of (a) Ce 3d in single-phase CeO_2, (b) Ce 3d in $Fe_3O_4/SiO_2/CeO_2$, (c) O 1s in single-phase CeO_2, (d) O 1s in $Fe_3O_4/SiO_2/CeO_2$, and (e) Fe 2p in $Fe_3O_4/SiO_2/CeO_2$.

X-ray photoelectron spectroscopy (XPS) was employed to characterize the chemical composition and valence state, as well as the shifted peaks in binding energies of the prepared samples, are shown in Fig. 3. The typical six peaks of Ce 3d were generated into three pair of spin orbit doublet. From the peaks denoted position, the Ce in the prepared samples were assigned to Ce^{4+} as corresponding with other reports [31, 32]. The comparison of the XPS spectra of Ce 3d between the Ce 3d in single-phase CeO_2 (Fig. 3a) and $Fe_3O_4/SiO_2/CeO_2$ core-shell magnetic nanoparticles (Fig. 3b) indicated that the peak position of these two samples was slightly different, possibly due to the chemical environment of two samples were not the same. In the region of Ce 3d in CeO_2 single-phase (Fig 3a), the binding energy was attributed to the Ce-O-Ce bond [33]. For Ce 3d in $Fe_3O_4/SiO_2/CeO_2$ core-shell sample, the binding energy decreased a little from the single-phase, which is due to the presence of Ce-O-Si bond. Since the oxygen presented the highest electronegativity as the following order; oxygen> silicon> cerium, thus more electrons from cerium atom could be transfer to oxygen, resulting in the decreased electron density on cerium atom in single-phase CeO_2 and caused the binging energy of Ce 3d shifted towards higher position [34, 35]. The results from this study probably confirmed the formation of Ce-O-Si bond in $Fe_3O_4/SiO_2/CeO_2$ sample. In the region of O 1s (Fig. 3c and 3d), the binding energy of O 1s in single-phase CeO_2 slightly increased from 529.50 eV to 529.72 eV for O 1s in $Fe_3O_4/SiO_2/CeO_2$ core-shell magnetic sample. Since Ce atom exhibited poor electron donating ability comparing with Si atom, therefore the O atom in CeO_2 single-phase (Ce-O-Ce bond) can induce more electrons from Ce atom than that of Si atom (Ce-O-Si bond), leading to the increased electron densities and low binding energy of O 1s atom was observed in the case of single-phase CeO_2 [36]. In order to confirm the valence state of Fe_3O_4 in core-shell composite sample, XPS spectra of the Fe 2p regions (Fig. 3e) were well deconvoluted by the peak denoted position of Fe $2p_{3/2}$ and Fe $2p_{1/2}$ corresponding to both Fe^{2+} and Fe^{3+} in Fe_3O_4. Since the binding energy of element increases with the increase of its valence state, thus the peak denoted position of Fe^{3+} is higher than Fe^{2+} as related to other reports [37, 38].

The morphology of single-phase CeO_2, Fe_3O_4/CeO_2, Fe_3O_4/SiO_2 and $Fe_3O_4/SiO_2/CeO_2$ core-shell magnetic nanoparticles were observed by HRTEM. As shown in Fig. 4a, it can be seen that CeO_2 single-phase has spherical morphology, and diameter is about 10 nm. HRTEM images in Fig. 4b show that Fe_3O_4 was formed by mixing with CeO_2 with the avearage diameters of 8–10 nm. It can be clearly seen from Fig. 4c that the Fe_3O_4/SiO_2 formed as the core-shell structure. The size of Fe_3O_4 core is about 20 nm and the outer layer distance of SiO_2 is in the range of 12–14 nm. The HRTEM images in Fig. 4d further confirmed

the $Fe_3O_4/SiO_2/CeO_2$ core shell structure that they consisted of three parts and the outer part is composed of many CeO_2 nanoparticles with the size of less than 10 nm.

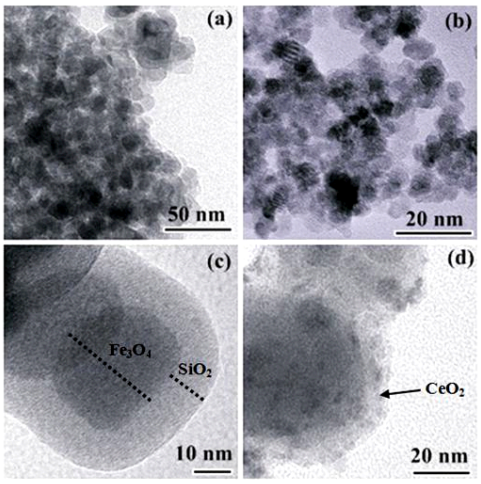

Fig. 4. HRTEM images of (a) single-phase CeO_2, (b) Fe_3O_4/CeO_2, (c) Fe_3O_4/SiO_2, and (d) $Fe_3O_4/SiO_2/CeO_2$ core-shell magnetic nanoparticles.

In order to estimate the band gap energies of the $Fe_3O_4/SiO_2/CeO_2$ core-shell magnetic nanoparticles, the optical properties were obtained from UV-Visible spectrometer with integrating sphere attachment. The Kubelka-Munk absorbance spectrum (Fig. 5b) was obtained from the reflectance spectra (Fig. 5a) using the Kubelka-Munk equation as follows [39]:

$$F(R_\infty)=(1-R_\infty)^2/2R_\infty \quad (1)$$

Where $F(R_\infty)$ and R_∞ are the Schuster-Kubelka-Munk absorbance and the absolute reflectance of the sample, respectively

The band gap energies of the obtained samples can be determined by using the intercept of the tangent to the graph plotting between the Kubelka-Munk absorption function and photon energy (hv) as shown in Fig. 5c. The obtained band gap energies (E_g) were determined to be 1.60 and 3.20 eV for Fe_3O_4 and CeO_2, respectively. Since the UV-Vis machine in this study is limited for the UV absorption detection below 200 nm, thus the large band gap of SiO_2 cannot be observed from this measurement.

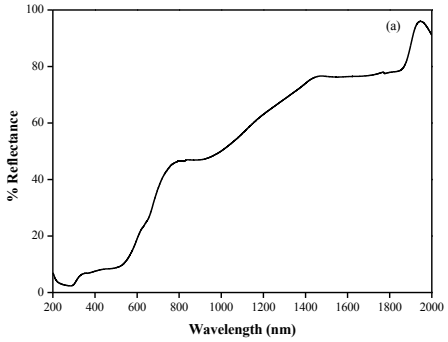

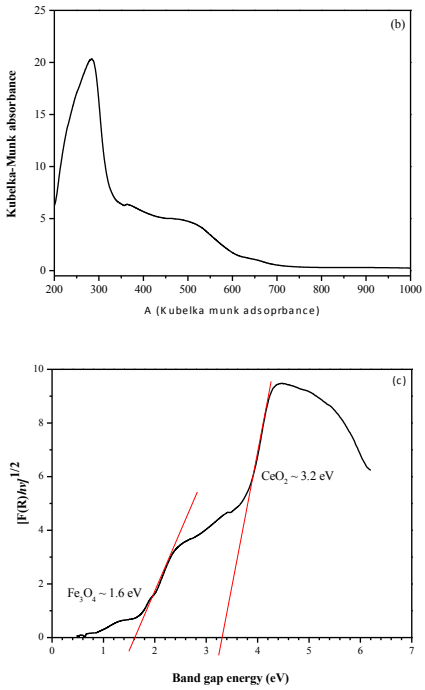

Fig. 5. UV-vis (a) reflection spectra, (b) absorbance Kubelka-Munk, and (c) relation between band gap energy and $[F(R)h\upsilon]^{1/2}$ of $Fe_3O_4/SiO_2/CeO_2$ core-shell magnetic nanoparticles with estimated band gap energies.

Based on the optical band gap energy values determined above (Fig. 5c) and equations below, the conduction band (CB) and valence band (VB) edge potentials of CeO_2 and Fe_3O_4 can be calculated [40]:

$$E_{cb}(CeO_2) = \chi\,(CeO_2) - E^C - \tfrac{1}{2}\,Eg \quad (2)$$

$$E_{cb}(CeO_2) = \chi\,(Fe3O4) - E^C - \tfrac{1}{2}\,Eg \quad (3)$$

$$E_{vb} = E_g - E_{cb}(CeO_2) \quad (4)$$

Where χ is the absolute electronegativity of CeO_2 (5.56 eV) [41] and Fe_3O_4 (5.78 eV) [42], E^C is the scaling factor relating the hydrogen electrode scale (NHE) to absolute vacuum scale (AVS) (~4.5 eV*vs.* AVS for 0 V *vs.*NHE) [40], and the estimated (Eg) of CeO_2 and Fe_3O_4 from the UV-vis plot are 3.2 and 1.6 eV, respectively.

The calculated positions of the valence band and the conduction bands of CeO_2 and Fe_3O_4 are listed in Table 1,

TABLE I. Conduction band potentials, valence band potentials,and band gap energies of CeO_2 and Fe_3O_4.

	CeO_2	**Fe_3O_4**
Conduction band potential (eV)	-0.54	0.48
Valence band potential (eV)	2.66	2.08
Band gap energy (eV)	3.20	1.60

In order to explained the effect of SiO_2 insulator middle layer on the prevented of electron-hole pair recombination at Fe_3O_4 core center, the electron-hole separation and charge transfer process was proposed based on the obtained HRTEM morphology and UV-Vis DRS results. From the HRTEM morpholody of Fe_3O_4/CeO_2 sample without SiO_2 inner layer, they presented a coupled semiconductor system by the two particles are in contact with each other. In coupled systems [43], UV light promoted electrons of CeO_2 excited from the valence band to the conduction band, and then separated hole and electron transported to the semiconductor interface, and react with adsorbed formic/oxalic acids molecules, see Fig. 6. The generated electron not only transferred to the CeO_2 surface but also injected into the lower conduction band of narrow band gap of Fe_3O_4 magnetic core (~1.6 eV) which may act as electron-hole recombination center [44], and might result in lower activities of couple system. Therefore the charge carriers cannot be utilized for redox reaction at catalyst surface during the photocatalytic reaction.

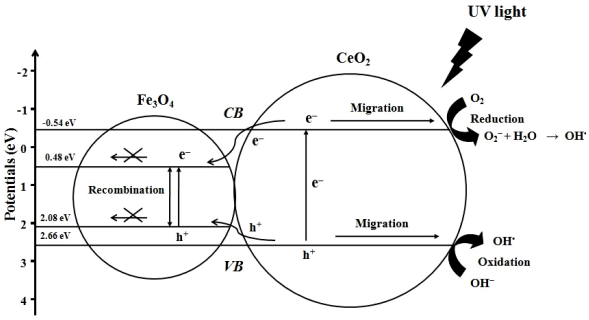

Fig. 6. Proposed mechanism for the photoexcited electron-hole separation and transport processes at the Fe_3O_4/CeO_2 couple under UV light irradiation.

In order to solve the problem on the electronic interactions at the Fe_3O_4/CeO_2, the SiO_2 middle layer is believed to help prevent the Fe_3O_4 from being as an electron-hole recombination center by blocking the electrons transfer from CeO_2 into the Fe_3O_4 core, which could help into a higher photoactivity [45,46]. The charge transfer processes involved in capped systems [47] of $Fe_3O_4/SiO_2/CeO_2$ core-shell structure is shown in Fig. 7. In a capped semiconductor system, the Fe_3O_4 and SiO_2 presented a core and shell geometry, respectively as confirmed from the HRTEM results, and both of them contacted with CeO_2 in a coupled semiconductor system. The two photogenerated electron and hole are accessible on the surface for oxidation and reduction processes. Then the generated hydroxyl radical OH• can react with adsorbed formic/oxalic acid, and finally generating H_2O and CO_2 as reaction products.

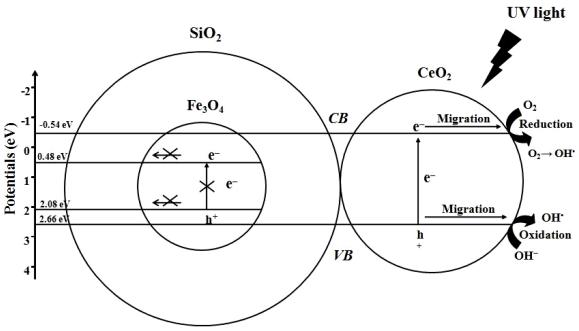

Fig. 7. Proposed mechanism for the photoexcited electron–hole separation and transport processes of the couple between CeO_2 and the capped Fe_3O_4/SiO_2 under UV light irradiation.

From Fig. 8 and Fig. 9, the kinetic data for formic and oxalic acids photoactivity under UV irradiation for 120 min were found to follow pseudo-first order reaction, and the equation is showed in equation (5) [48].

$$-\ln (C/C_0) = kt \qquad (5)$$

where k is the apparent rate constant (min^{-1}), C_0 means the initial concentration of acid and C refers the concentration of acid at various contact times (t).

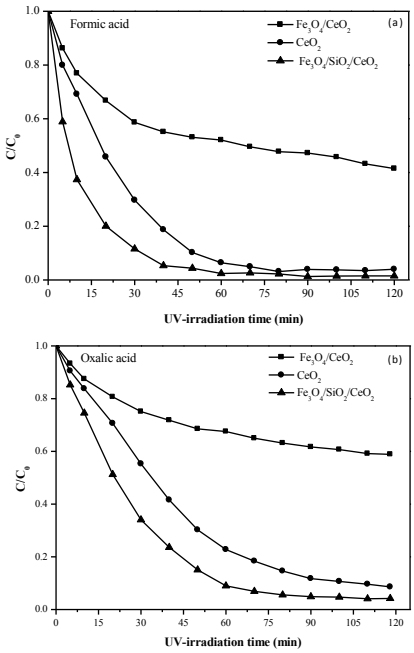

Fig. 8. Photocatalytic degradation of (a) formic acid and (b) oxalic acid by Fe_3O_4/CeO_2, CeO_2, and $Fe_3O_4/SiO_2/CeO_2$ core-shell magnetic nanoparticles as a function of UV light irradiation time.

The plot results reported based on the amount of carbon dioxide generated as the reaction proceeded. From the photoactivity results of formic acid (Fig. 8a) and oxalic acid (Fig. 8b), it can be concluded that the photocatalytic activity of the CeO_2 directly deposited onto Fe_3O_4 core (Fe_3O_4/CeO_2) was lower than that of single-phase

CeO_2. The improvement in photoactivity was achieved over the $Fe_3O_4/SiO_2/CeO_2$ core-shell structure, which direct contact between the CeO_2 and the Fe_3O_4 core was prevented by SiO_2 middle layer. For comparison, the results of the photocatalytic activity revealed that apparent rate constant for formic acid (Fig. 9a) and oxalic acid (Fig. 9b) degradation was increased in the following order; $Fe_3O_4/SiO_2/CeO_2$ core-shell magnetic nanoparticles> single-phase CeO_2> Fe_3O_4/CeO_2.

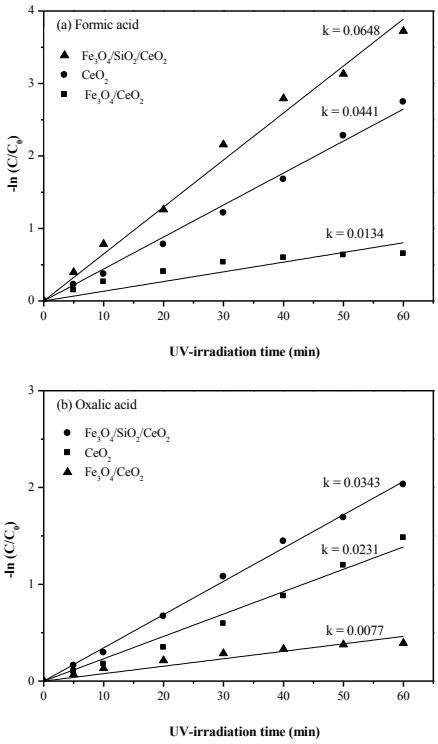

Fig. 9. Kinetics plots for linear fitting of data obtained from pseudo first order reaction for (a) formic acid and (b) oxalic acid degradation under UV light.

Another reason for the good photocatalytic activity of $Fe_3O_4/SiO_2/CeO_2$ core-shell magnetic nanoparticles is due to their high specific surface area and large average pore size diameter (Table 2), which provided more efficiency for photocatalytic activity by not only adsorbing more formic or oxalic acid molecules but also offering more reaction sites [49].

TABLE II. The surface properties of the single-phase CeO_2 and $Fe_3O_4/SiO_2/CeO_2$ core-shell magnetic nanoparticles.

	Single-phase CeO_2	$Fe_3O_4/SiO_2/CeO_2$ core-shell magnetic nanoparticles
Surface area (m^2/g)	62.20	65.10
Pore volume (cm^3/g)	0.14	0.43
Average pore size (nm)	4.20	13.30

Since the important real world consideration for photocatalytic systems is long-term stability, therefore the reusability of the catalyst was studied over the $Fe_3O_4/SiO_2/CeO_2$ core-shell magnetic nanoparticles. After the raction finished, the core-shell magnetic catalyst was recovered by applying the external magnet, and washed with distilled water. The regenerated magnetic core-shell catalyst was reused again for the next formic and oxalic acids degradation run. It was found that the process was repeated for three cycles in total and presented a good stability with regards to photocatalytic performance, with less than 10% decrease from its initial activity during process (Fig. 10). Thus, $Fe_3O_4/SiO_2/CeO_2$ core-shell magnetic nanoparticlescan be used as effective and convenient recyclable photocatalysts.

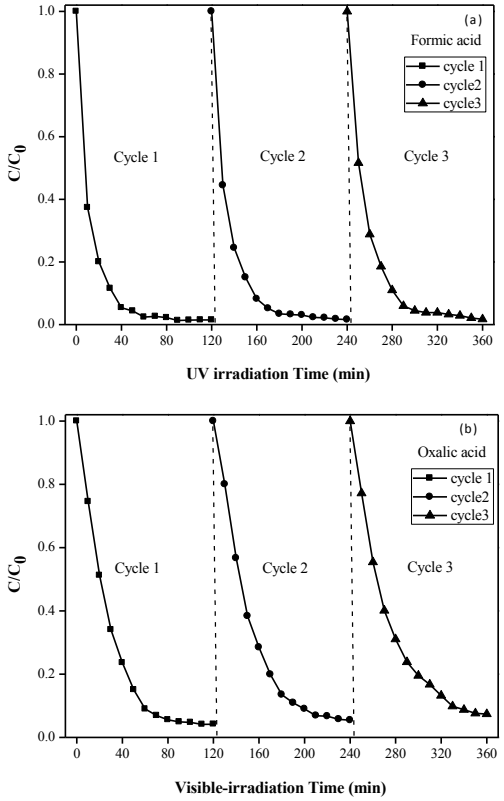

Fig. 10 . Cycling runs of (a) formic acid and (b) oxalic acid over $Fe_3O_4/SiO_2/CeO_2$ core-shell magnetic nanoparticles under UV irradiation.

The remaining CeO_2 phase in core-shell structure was also checked by XRD technique after core-shell magnetic catalyst was recovered at the end of each experimental. Since the CeO_2 outer layer act as a main photocatalysts to degrade formic and oxalic acids in wastewater, therefore the phase remaining confirmation of CeO_2 is necessary for another cycle of an experiment. As shown in Fig. 11, XRD patterns still remained the CeO_2 phase in core-shell catalyst after recovering from the treated suspension.

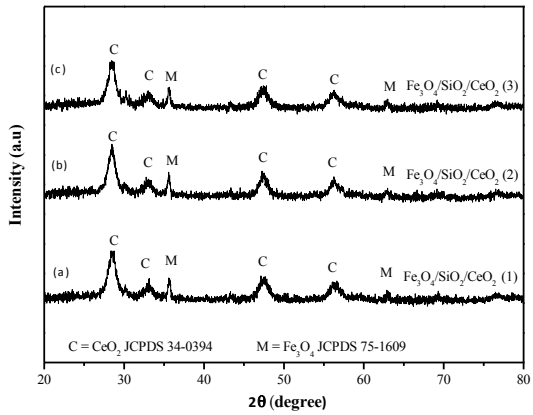

Fig. 11. The XRD patterns of Fe3O4/SiO2/CeO2 core-shell magnetic nanoparticles (a) after the first run (b) after the second run, and (c) after the third run.

VI. Conclusions

In summary, $Fe_3O_4/SiO_2/CeO_2$ core-shell magnetic nanoparticles, which are capable of fast magnetic separation have been successfully synthesized by combining three steps of the hydrothermal, sonochemical and the homogeneous precipitation. The prepared core-shell structure was composed of Fe_3O_4 magnetic core with a strong response to external magnet, the SiO_2 middle layer, and an outer part of CeO_2 nanoparticles. The presence of SiO_2 makes it possible to achieve higher photocatalytic efficiency than that of the Fe_3O_4/CeO_2 and single-phase CeO_2. The highest specific surface area, pore volume and pore size diameter of $Fe_3O_4/SiO_2/CeO_2$ core-shell magnetic nanoparticles could be provided more surface active sites for the adsorption of formic and oxalic acids molecules, causing the higher efficiency in photocatalytic activity. The experimental demonstrated that $Fe_3O_4/SiO_2/CeO_2$ core-shell magnetic nanoparticles can be easily recycled by applying an external magnetic field while maintaining their photocatalytic activity during at least three cycles of use. The morphology from HRTEM images and the band edge position (DRS UV-Vis) were employed to propose the mechanism for the photoexcited electron-hole separation and transport processes over the coupled system (Fe_3O_4/CeO_2) and capped system ($Fe_3O_4/SiO_2/CeO_2$) under UV light irradiation. Therefore reusability of the magnetic catalyst is one of the best efficient economically recycling.

Acknowledgment

This work has been supported by Thailand Research Fund (TRF) through the Royal Golden Jubilee (RGJ)-Ph.D Program. National Research University Project under Thailand's Office of Higher Education Commission; Materials Science Research Center, Department of Chemistry, Faculty of Science and the Graduate School, Chiang Mai University are greatly acknowledged.

References

[1] R. Andreozzi, V. Caprio, A. Insola, R. Marotta, "Advanced oxidation processes (AOPs) for water purification and recovery," Catal. Today., vol. 53, pp. 51–59, October 1999.

[2] L. W. Perelo, "Review: in situ and bioremediation of organic pollutants in aquatic sediments," J. Hazard. Mater., vol. 177, pp. 81–89, May 2010.

[3] K. H. Wang, Y. H. Hsieh, M. Y. Chou, C. Y. Chang, "Photocatalytic degradation of 2-chloro and 2-nitrophenol by titanium dioxide suspensions in aqueous solution," Appl. Catal. B Environ., vol. 21, pp. 1–8, May 1999.

[4] F. Akbal, A. N. Onar, "Photocatalytic degradation of phenol," Environ. Monit. Assess., vol. 83, pp. 295–302, April 2003.

[5] B. Ozkaya, Adsorption and desorption of phenol on activated carbon and a comparison of isotherm models, J. Hazard. Mater. 129 (2006) 158–163.

[6] K. H. Lanouette, "Treatment of phenolic wastes," Chem. Eng. J., vol. 17, pp. 99–106, October 1997.

[7] S. Bang, M. Patel, L. Lippincott, "Removal of arsenic from groundwater by granular titanium dioxide adsorbent," Chemosphere., vol. 60, pp. 389–397, July 2005.

[8] T. V. Gerven, G. Mul, J. Moulijn, A. Stankiewicz, "A review of intensification of photocatalytic processes," Chem. Eng. Process., vol. 46, pp. 781–789, September 2007.

[9] A. L. Linsebigler, G. Lu, J. T. Yates, "Photocatalysis on TiO2 surfaces: principles, mechanisms and selected results," Chem. Rev., vol. 95, pp. 735–758, May 1995.

[10] M. G. Neelavannan, M. Revathi, C. Ahmed Basha, "Photocatalytic and electrochemical combined treatment of textile wash water," J. Hazard. Mater., vol. 149, pp. 371–378, October 2007.

[11] P. K. J. Robertson, "Semiconductor photocatalysis: an environmentally acceptable alternative production technique and effluent treatment process," J. Cleaner Prod., vol. 4, pp. 203–212, November 1997.

[12] L. Chen, J. Tian, H. Qiu, "Preparation of TiO2 nanofilm via sol-gel process and its photocatalytic activity for degradation of methyl orange," Ceram. Int., vol. 13, pp. 3422–3435, December 2009.

[13] S. W. Kim, H. K. Kim, H. W. Choi, D. H. Yoo, E. J. Kim, S. H. Hahn, "Photocatalytic activity of metal-inserted WO3 thin films prepared by RF magnetron sputtering," J. Nanosci. Nanotechnol., vol. 10, pp. 7053–7055, October 2013.

[14] W. Shen, Z. Li, H. Wang, Y. Liu, Q. Gu, Y. Zhang, "Photocatalytic degradation for methylene blue using zinc oxide prepared by codeposition and sol-gel methods," J. Hazard. Mater., vol. 152, pp. 172–175, March 2008.

[15] L. Truffault, M. Ta, T. Devers, K. Konstantinov, C. Harel, C. Simmonard, C. Andreazza, I. P. Nevirkovets, A. Pineau, O. Veron, J. P. Blondeau, "Application of nanostructured Ca doped CeO2 for ultraviolet filtration," Mater. Res. Bull., vol. 45, pp. 527–535, March 2010.

[16] Y. Gao, W. Wang, S. Chang, W. Huang, "Morphology effect of CeO2 support in the preparation, metal–support interaction, and catalytic performance of Pt/CeO2 catalysts," Chem. Cat. Chem., vol. 5, pp. 3610–3620, December 2013.

[17] R. G. Ranga, B. G. Mishra, "Structural, redox and catalytic chemistry of ceria based materials," J. Indian. Chem. Soc., vol. 2, pp. 122–134, 2003.

[18] Z. Wang, Y. Guo, S. Li, Y. Sun, N. He, "Synthesis and characterization of SiO2/(PMMA/Fe3O4) magnetic nanocomposites," J. Nanosci. Nanotechnol., vol. 8, pp.

1797–1802, April 2008.

[19] R. Watts, S. Kong, W. Lee, “Sedimentation and reuse of titanium dioxide: application to suspended-photocatalyst reactor,” J. Environ. Eng., vol. 7, pp. 730–735, October 1995.

[20] T. Kemmitt, N. I. Al-Salim, M. Waterland, V. J. Kennedy, A. Markwitz, “Photocatalytictitania coatings,” Curr. Appl. Phys., vol. 4, pp. 189–192, April 2004.

[21] D. I. Petkowicz, R. Brambilla, C. Radtke, C. D. S. Silva, Z. N. Rocha, S. B. C. Pergher, J. H. Z. Santos, “Photodegradation of methylene blue by in situ generated titania supported on a NaA zeolite,” Appl. Catal. A., vol. 357, pp. 125–134. April 2009.

[22] L. K. Tan, M. K. Kumar, H. Gao, “Transparent, well-aligned TiO2 nanotube arrays with controllable dimensions on glass substrates for photocatalytic applications,” ACS Appl. Mater. Interface., vol. 2, pp. 498–503, February 2010.

[23]. D. G. Shchukin, A. I. Kulak, D. V. Sviridov, “Magnetic photocatalysts of the core-shell type,” J. Photochem., vol. 10, pp. 742–744, September 2002.

[24] K. F. Yao, Z. Peng, Z. H. Liao, J. J. Chen, “Preparation and photocatalytic property of TiO2-Fe3O4 core-shell nanoparticles,” J. Nanosci. Nanotechnol., vol. 9, pp. 1458–1461, February 2009.

[25] F. Caruso, R. A. Caruso, H. M. Öhwald, “Nanoengineering of inorganic and hybrid hollow spheres by colloidal templating,” Science., vol. 282, pp. 1111–1114, November 1998.

[26] G. Li, Q. Shi, S. J. Yuan, K. J. Neoh, E. T. Kang, X. Yang, “Alternating silica/polymer multilayer hybrid microspheres templates for double-shelled polymer and inorganic hollow microstructures,” J. Mater. Chem., vol. 22, pp. 1309–1317, January 2010.

[27] A. Khare, R. J. Choudhary, K. Bapna, D. M. Phase, S. P. Sanyal, “Resonance photoemission studies of (111) oriented CeO2 thin film grown on Si (100) substrate by pulsed laser deposition,” J. Appl. Phys., vol. 108, pp. 1–5, November 2010.

[28] R. Wang, C. Wang, W. B. Cai, “Ultralow platinum loading high performance nanoporouselectrocatalysts with nanoengineered surface structures,”Adv. Mater., vol. 22, pp. 1845–1848, April 2010.

[29] S. Zhao, D. K. Lee, C. W. Kim, H. G. Cha, Y. H. Kim, Y. S. Kang, “Synthesis of magnetic nanoparticles of Fe3O4 and CoFe2O4 and their surface modification by surfactant adsorption,” Bull. Kor. Chem. Soc., vol. 27, pp. 237–242, July 2005.

[30] G. Basina, G. Mountrichas, E. Devlin, N. Boukos, D. Niarchos, D. Petridis, S. Pispas, V. Tzitzios, “Synthesis and magnetic properties of Fe3O4 nanoparticles coated with biocompatible double hydrophilic block copolymer,” J. Nanosci. Nanotechnol., vol. 9, pp. 1–7, August 2009.

[31] K. M. Joshi, V. S. Shrivastava, “Removal of methylene blue dye aqueous solution using photocatalysis”, Int. J.NanoDimens., vol. 2, pp. 241–252, April 2012.

[32] K. P. Gajendra, K. M. Parida, “Fabrication of iron-cerium mixed oxide: an efficient photocatalyst for dye degradation,” Int. J. Appl. Sci. Eng. Tech., vol. 2, pp. 53–65, August 2010.

[33] A. Gupta, U. V. Waghmare, M. S. Hegde, “Correlation of oxygen storage capacity and structural distortion in transition-metal, noble-metal, and rare-earth-ion-substituted CeO2 from first principles calculation,” Chem. Mater., vol. 22, pp. 5184–5198, August 2010.

[34] E. J. Preisler, O. J. Marsh, R. A. Beach, T. C. McGill, “Stability of cerium oxide on silicon studied by x-ray photoelectron spectroscopy,” J. Vac. Sci. Tech. B., vol. 19, pp. 1611–1618, January 2001.

[35] K. B. Sundaram, P. F. Wahid, O. Melendez, “Deposition and x-ray photoelectron spectroscopy studies on sputtered cerium dioxide thin films,” J. Vac. Sci. Tech., vol. 15, pp. 52–56, October 1996.

[36] A. Tarek, K. Fujimura, S. Kato, S. Satokawa, T. Kojima, “Preparation and characterization of magnetically separable photocatalyst (TiO2/SiO2/Fe3O4): effect of carbon coating and calcination temperature,” J. Hazard. Mater., vol. 154, pp. 572–577, June 2008

[37] A. P. Grosvenor, B. A. Kobe, M. C. Biesinger, N. C. McIntyre, “Investigation of multiplet splitting of Fe 2p XPS spectra and bonding in iron compounds,” Surf. Interface. Anal., vol. 36, pp. 1564–1574, December 2004.

[38] T.Yamashita, P. Hayes, “Analysis of XPS spectra of Fe2+ and Fe3+ ions in oxide materials,” Appl. Surf. Sci., vol. 254, pp. 2441–2449, February 2008.

[39] J. Sirita, S. Phanichphant, F. C. Meunier, “Quantitative analysis of adsorbate concentrations by diffuse reflectance FT-IR,” Anal. Chem., vol. 79, pp. 3912–3918, April 2007.

[40] Y. Xu, M. A. Schoonen, “The absolute energy position of conduction and valence bands of selected semiconducting minerals,” Am. Mineral. J., vol. 85, pp. 543–556, 2000.

[41] G. Magesh, B. Viswanathan, R. P. Viswanath, T. K. Varadarajan, “Photocatalytic behavior of CeO2-TiO2 system for the degradation of methylene blue,” Indian. J. Chem. Tech., vol. 48, pp. 480−488, April 2009.

[42] R. G. Pearson, “Absolute electronegativity and hardness: application to inorganic chemistry,” Inorg. Chem., vol. 27, pp. 734–740, February 1988.

[43] I. Bedja, P. V. Kamat, “Photosensitization of composite semiconductor based nanocrystalline semiconductor films,” J. Chem. Phys., vol. 99, pp. 9182–9188, November 1997.

[44] X. Huang, G. Wang, M. Yang, W. Guo, H. Gao, “Synthesis of polyaniline-modified Fe3O4/SiO2/TiO2 composite microspheres and their photocatalytic application,” Mater. Lett., vol. 65, pp. 2887–2890, October 2011.

[45] T. A. Gad-Allah, S. Kato, S. Satokawa, T. Kojima, “Treatment of synthetic dyes wastewater utilizing a magnetically separable photocatalyst (TiO2/SiO2/Fe3O4): parametric and kinetic studies,” Solid State Sci., vol. 244, pp. 1–11, August 2009.

[46] Z. Wang, S. Zhu, S. Zhao, H. Hu, “Synthesis of core–shell Fe3O4@SiO2@MS (M= Pb, Zn, and Hg) microspheres and their application as photocatalysts,” J. Alloy Comp., vol. 509, pp. 6893–6898, June 2011.

[47] D. Beydoun, R. Amal, S. McEvoy, “Novel photocatalyst: titania-coated magnetite : activity and photodissolution,” J. Phys. Chem. B., vol. 104, pp. 4387–4396, April 2000.

[48] A. Olad, S. Behboudi, A. A. Entezami, “Preparation, characterization and photocatalytic activity of TiO2/polyaniline core-shell nanocomposite,” Bull. Mater. Sci., vol. 35, pp. 801–809, October 2012.

[49] D. Channei, B. Inceesungvorn, N. Wetchakun, S. Phanichphant, “Kinetics study of photocatalytic activity of flame-made unloaded and Fe-loaded C eO2 nanoparticles,” Int. J. Photoenergy., vol. 2013, pp. 1–9, October 2013.